

# **Modeling Stream Hydraulics Before and After a Meander Restoration Project**

BY

JOSE JAVIER MARQUEZ REINA  
B.S. University of Seville, Spain 2003  
M.S. University of Cordoba, Spain 2008

THESIS

Submitted as partial fulfillment of the requirements  
for the degree of Master of Science in Civil Engineering  
in the Graduate College of the  
University of Illinois at Chicago, 2017

Chicago, Illinois

Defense Committee:

Sybil Derrible, Chair  
Sean Vitousek, Advisor  
Ben O'Connor, U.S. Army Corps of Engineers

## **ACKNOWLEDGEMENTS**

I would like to thank my thesis committee - Sybil Derrible, Sean Vitousek and Ben O'Connor - for their support and assistance throughout this process.

Scott LaVanne and John Wills with WBK Engineering and Scott Meister and Jessi DeMartini with DuPage County Forest Preserve were extremely patient in answering my numerous questions and providing data and documents vital to my study. I'd also like to thank Abhilasha Rajesh and Nick Haas in helping with data collection at Spring Brook.

JJMR

## TABLE OF CONTENTS

SECTION		PAGE
1.	INTRODUCTION.....	1
2.	SITE DESCRIPTION.....	5
3.	METHODS.....	9
3.1.	Field Data Collection.....	9
3.2.	Numerical Model.....	12
3.3.	Rating Curves: Model Calibration.....	17
3.3.1.	Downstream Rating Curves.....	18
3.3.2.	Upstream Rating Curves.....	24
4.	RESULTS.....	26
4.1.	Model Validation.....	26
4.2.	Continuous flow depth and flow rate readings.....	27
5.	DISCUSSION.....	31
6.	CONCLUSIONS.....	41
	REFERENCES.....	43
	APPENDIX.....	47
	VITA.....	49

## LIST OF TABLES

<b>TABLE</b>		<b>PAGE</b>
I.	WATERSHED CHARACTERISTICS.....	5
II.	ORIGINAL AND RESTORED STREAM CONDITIONS.....	8
III.	DATES AND LOCATION OF DATA COLLECTION.....	11
IV.	COLLECTED DISCRETE FIELD DATA AND FLOW FREQUENCY ANALYSIS RESULTS.....	16
V.	MANNING'S ROUGHNESS NUMBER OPTIMIZED FOR THE MODELING WORK.....	20

## LIST OF FIGURES

<b>FIGURE</b>		<b>PAGE</b>
1.	Watershed delimitation.....	6
2.	Aerial photographs of the pre-restoration and restored study stream reaches geomorphology.....	7
3.	Field work and instruments.....	10
4.	Pre-restored and restored reaches GIS layers.....	15
5.	Downstream rating curves used for model calibration and estimation of flow rates based on direct measurements of flow depth.....	19
6.	Rectangular and trapezoidal open channel geometry.....	21
7.	Stage-discharge relationship for an ideal rectangular and trapezoidal stream channel.....	23
8.	Upstream rating curves used for model calibration.....	24
9.	Model validation for the downstream data collection site.....	26
10.	Model validation for the upstream data collection site.....	27
11.	Continuous flow depth for the two data collection sites.....	28
12.	Continuous flow rate determined at the downstream data collection site.....	29
13.	Flood maps for the pre-restored and the restored stream configurations.....	32
14.	Probability distribution for hydraulic variables before and after stream restoration.....	35
15.	Joint probability distribution of water depth and flow velocity for the pre-restored and the restored stream configurations.....	37
16.	Comparison of preferred ranges of flow depth and velocity for invertebrates, pearl mussels and green sunfish with Spring Brook's depth and velocity conditions (before and after restoration).....	39
17.	Return frequency analysis for Spring Brook.....	48

## LIST OF ABBREVIATIONS

1D	One-Dimensional
2D	Two-Dimensional
ADV	Acoustic Doppler Velocimeter
DS	Downstream
DTM	Digital Terrain Model
GIS	Geographic Information System
H	Flow Depth
LIDAR	Light Detection and Ranging
Q	Flow Rate
Tr	Return Period
V	Flow Velocity
XS	Cross-section

## SUMMARY

This study models the stream hydraulics before and after a meander restoration project completed in 2015 at Spring Brook near Wheaton, Illinois. Field work was carried out during 2016 and 2017 in order to collect data (continuous flow depth from two permanently installed sondes as well as discrete flow depth and flow rate from an Acoustic Doppler Velocimeter).

A HEC-RAS model was built based on geospatial data of the pre- and post- restoration stream configurations prepared using HEC-GeoRAS. The model was calibrated with the discrete data collected in the field. In the calibration and validation process, stage-discharge relationships (rating curves) were derived as means for obtaining discharge records from direct observations of flow depth.

The rating curves were applied to the continuous flow depth data collected in the field in order to obtain continuous discharge estimates. Then, the HEC-RAS and HEC-GeoRAS models were used to simulate normal and extreme flood conditions in the stream channel and floodplain, observing that the restored stream provides continuous hydraulic interaction between the channel and the floodplain for base flow conditions and higher, as opposed to the pre-restored stream, which requires much higher flow rates.

The HEC-RAS simulations of discrete flow events observed in the field provided a variety of hydraulic variables of interest, including flow depth, flow velocity, shear stress and stream power. We observed that the restored stream presents a wider variety of flow depth as a consequence of the construction of deep pools. Flow velocities were slightly reduced due to the lower slope of the new channel and the added meanders and deep pools. Shear stress and stream power were also slightly reduced in the restored case.

## **SUMMARY (Continued)**

When analyzing the co-located flow depth and flow velocity we observe two main regions of physical conditions with higher frequency of occurrence, as well as transition sections in between. This variability can be beneficial for the establishment of new habitats and species richness improvement as opposed to the uniform conditions in the pre-restored case.

## 1. INTRODUCTION

“If water is the essential ingredient of life, then water supply is the essential ingredient of civilization” (Sedlak, 2014). For centuries, humans have engineered watersheds in order to suit their needs, and in the process, have caused numerous impacts to the environment. The most severe impacts to aquatic systems in North America, Europe and elsewhere occurred since the industrial revolution, particularly in the 19th and 20th centuries (Roni and Beechie, 2013, Wohl et al., 2017). These impacts include dredged and channelized streams, drained wetlands, deforestation, mining and other extraction industries, intensified agriculture, and building dams for power, drinking water supply, irrigation, and flood control (Waal, et al., 1998; Roni and Quimby, 2005; Roni and Beechie, 2013). In the past few decades, a conservationist movement has appeared which sought numerous restoration projects (Simon et al., 2011) in attempt to promote the recovery of ecosystems that have been harmed in some degree by human activities (Society of Ecological Restoration, 2004).

Stream restoration is highly conditioned by environmental policy in the United States (Bronner et al., 2013; Doyle and Shields, 2012). Under the Rule for Compensatory Mitigation for Losses of Aquatic Resources, published in 2008, any development or activity that causes the inevitable loss of stream physicochemical or biological processes (function) must be compensated through the restoration or preservation of water resources (Palmer and Hondula, 2014). Nevertheless, this rule has been criticized for not specifying a design methodology, but instead relying on local U.S. Army Corps of Engineers office criteria, using key terminology ambiguously and giving more value to the quantity of restored ecosystems than quality (Bronner et al., 2013). Stream restoration is also driven primarily by flood control, mainly through flood peak discharge attenuation, although the ultimate objective should be the recovery of habitat and local fish population (Doyle and Shields, 2012).

Stream restoration projects are becoming well-established means for alleviating the effects of urbanization (Walsh et al., 2005). A main operating assumption of stream restoration is that returning channel configuration to its pre-degradation state will recuperate native aquatic biodiversity; however, many studies have shown that this is not always the case (Palmer et al., 2010; Violin et al. 2011). Stream restoration projects include: (a) re-establishing favorable temperatures, water quality, and habitats for aquatic species that thrive in those conditions, (b) replanting aquatic or riparian vegetation, (c) modifying stream width, depth, or meanders to re-balance stream velocity and sediment load, (d) building riffles or small structures in the upper watershed gullies to reduce headwater erosion and stabilize watersheds, and (e) improving stream banks so that they remain stable during periods of high flows during storms (Riley, 1998).

Achieving stream restoration is a complicated endeavor, in part because the relationship between stream hydraulics and stream ecology is poorly understood (Waal et al., 1998; ASCE River Restoration Subcommittee on Urban Stream Restoration, 2003). There are two schools of thought. The first one is the Natural Channel Design method popularized by David Rosgen, which is based on a reach form classification as means to assess the past, present and possible future channel behavior, assuming conditions do not change (Doyle et al., 1999); however, although commonly used, this method has been widely criticized and is only recommended for initial characterization and communication (Bronner et al., 2013; Doyle et al., 1999; Simon et al., 2007). The second approach consists of process-based methods that provide understanding of channel behavior focusing on the geomorphic processes that govern the equilibrium between forces and resistance (Simon et al., 2007)

Violin et al. (2011) demonstrated that small, reach-scale restoration projects may be incapable of reversing the large-scale effects of watershed urbanization. In contrast, they also suggested that superior restoration design and results would be achievable by expanding

restoration plans to address watershed-scale impacts. Another difficulty associated with achieving stream restoration is that many restoration projects are often inadequately monitored following completion because of insufficient funding or difficulty in planning and implementation (Roni & Quimby, 2005). In general, stream restoration is a multidisciplinary field that requires the contribution and close cooperation of diversified specialists, including geomorphologists, hydrologists, ecologists, civil engineers, landscape architects and planners, in order to create, implement, and monitor successful restoration projects (Waal et al., 1998).

The purpose of this study is to analyze and evaluate changes in stream hydraulics due to a meander restoration project completed in 2015 at Spring Brook in Wheaton, Illinois. Meander restoration is an increasingly popular stream restoration method consisting of the re-configuration of meanders in typically straight channelized stream reaches (Rinaldi and Johnson, 1997; Darby and Sear, 2008; Palmer et al., 2010). The goals of meander restoration include dissipation of excess flow energy, channel stabilization, reduction of transport capacity to moderate sediment discharge downstream from the restored reach, and promotion of habitat recovery (Rinaldi and Johnson, 1997).

Straight channelized streams generally pose less hydraulic resistance due to typically steeper slopes, higher flow velocities, and increased sediment transport compared to meandering streams (Doyle & Shields, 2012; Gore, 1985). From a habitat standpoint, meandering streams often provide wider ranges of flow depths, with deeper sections at the meander tip where bank erosion and scour occur, which can provide rearing, resting and cover areas for fish, as well as shallower regions of fast flows favorable for certain invertebrates (Cushing & Allan, 2001; Gore, 1985).

Degraded stream channels are characterized by limited hydraulic connection between the channel and the floodplain (Booth et al., 2001; Simon et al., 2011; Roni & Beechie, 2013; Booth & Fischenich, 2015). Therefore, an important benefit that can be derived from meander restoration is the reconnection of both stream channel and floodplain for a wide range of flow rates (Wohl et al., 2005). Additionally, flow storage and energy dissipation of flood events can be improved by meander restoration (Sholtes and Doyle, 2011).

The overall objective of this study is to determine how hydraulic modeling can assist in comparing the pre- and post-restoration stream channel hydraulics in Northeastern Illinois and evaluating the restoration objectives. A combination of field work and modeling is the basis for this analysis. Field data have been collected during 2016 and 2017 on the restored reach in order to validate a model (HEC-RAS) of the stream. No field data is available for the pre-restoration channel, and thus the model is applied to the pre-restoration stream once we have demonstrated the model's capability to accurately simulate the hydraulics of the restored reach.

## 2. SITE DESCRIPTION

In 2015, the Illinois Tollway, in partnership with the Forest Preserve District of DuPage County, DuPage County Division of Stormwater Management, The Wetlands Initiative, and WBK Engineering, completed a restoration project at Spring Brook, a first-order stream draining into the West Branch of DuPage River, tributary to the Des Plains River. This restoration project is part a major mitigation plan derived from the construction of the Elgin O'Hare Western Access project.

The study site is located 50 km west of Chicago, near the City of Wheaton, Illinois and extends within the St. James Farm Forest Preserve. The drainage basin has a total area of 15.62 km<sup>2</sup> with 91.80 % of developed area and 28.50% of impervious area (Table I and Figure 1). The average annual rainfall for this area is 935 mm per year, determined based on records obtained between the years 1895 to 2011 from a station near Wheaton, IL (data obtained from <https://www.ncdc.noaa.gov/cdo-web/datasets> using station GHCND:USC00119221).

**TABLE I. WATERSHED CHARACTERISTICS**

<b>Parameter</b>	<b>Value</b>
Perimeter	33.38 km
Length (from outlet to watershed divide)	9.77 km
Slope	0.12 %
Surface area	15.62 km <sup>2</sup>
Developed (urban) surface area	91.80 %
Average percentage of impervious area	28.50 %
Average soil permeability	24.92 mm/h
Percent of open water and herbaceous wetland	0.87 %

Source: U.S. Geological Survey (<https://streamstats.usgs.gov/ss>).

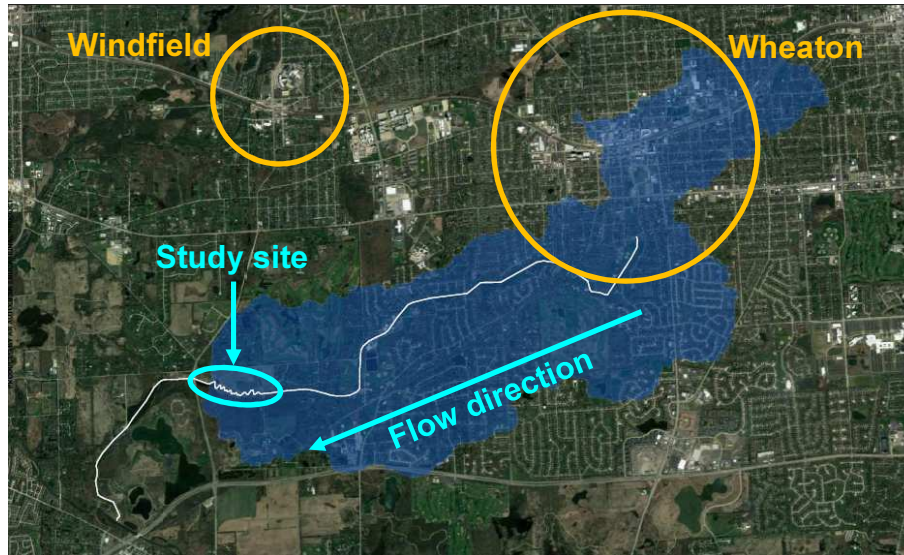


**Figure 1.** Watershed delimitation. Aerial imagery obtained from Google Earth.

Before agricultural and urban development in the surrounding area, Spring Brook was likely an intermittent or ephemeral prairie stream. However, Spring Brook is currently a perennial stream as a consequence of the continuous effluent discharge from the Wheaton Sanitary District Wastewater Treatment Plant, located approximately 1.2 kilometers upstream from the restoration site, which serves a population of over 60,000 people and has a design average of 33,700 m<sup>3</sup>/d (Illinois Tollway, 2014), which represents approximately 90% of the observed base flow conditions.

Over the past century, local farmers and developers deepened and straightened the stream, which lowered the channel and eliminated the stream's lateral connection with the floodplain (Illinois Tollway, 2014). The Illinois Environmental Protection Agency (2014), in compliance with the Clean Water Act, included Spring Brook in the 303(d) impaired waters list for not allowing aquatic life and primary contact recreation (e.g. complete submergence activities, like swimming). The principle limitations on aquatic diversity at Spring Brook were due

to the lack of gravel substrates, poor bank conditions and stream sinuosity, and homogenized flow conditions (Illinois Tollway, 2014).

The main geomorphological feature of the restoration project is the stream re-configuration into a meandering alignment (Figure 2). The restoration project also included the addition of in-stream sequences of pools and riffles. Additionally, diverse wetland habitats were restored within the floodplain, for some of which portions of the abandoned straightened steam channel were used. The restored channel is 329 m longer, with a slightly smaller slope (0.04%), an increased sinuosity (1.53) and better distributed bed material including coarse gravel, cobbles and some boulders (Table II).



**Figure 2.** Aerial photographs of (A) pre-restoration (2013) and (B) restored (2017) study stream reach geomorphology. Aerial imagery obtained from Google Earth.

**TABLE II. ORIGINAL AND RESTORED STREAM CONDITIONS**

	<b>Pre-restored reach</b>	<b>Restored reach</b>
Channel length	697.16 m	1025.66 m
Channel slope	0.07%	0.04%
Sinuosity <sup>1</sup>	1.05	1.53
Channel geometry	Width to depth ratio: 6.5	Width to depth ratio: 15.7
Bed material	Fine sediments over armored gravel. $D_{50} = 9.6$ mm (medium gravel) <sup>2,3</sup>	Combination of silt deposits in low velocity sections and very coarse gravel and fine to coarse cobble in high velocity sections with some fine boulder. $D_{50} = 13.7$ to 26.9 mm (coarse gravel) <sup>2,3</sup>

<sup>1</sup> Sinuosity determined as the channel length within the upstream and downstream boundaries divided by the straight line distance between the boundary locations.

<sup>2</sup> Wolman pebble counts carried out by WBK Engineering (Paver and Olson, 2017).

<sup>3</sup> Buffington and Montgomery (1999).

The restoration project objectives described by the Illinois Tollway 2014 report include flow energy dissipation, erosion reduction, stream velocity slowdown, channel and floodplain reconnection and wetland recovery. Additionally, the restoration project sought promotion of a variety of flow velocity/depth regimes and functional aquatic habitats intended to increase the diversity and abundance of fish and macroinvertebrate species, with the focus on mussels for their nutrient cycling capacity (Hoellein et al., 2017).

### 3. METHODS

A combination of regular field data collection and numerical modeling has been used as the basis for the hydraulic analysis and comparison between the pre-restoration and the restored stream configurations. The field data is used to calibrate and validate the numerical model, and therefore extend the spatiotemporal range of hydraulic conditions at Spring Brook, beyond the limited range of flow conditions observed at isolated locations and discrete times during field work. Due to difficulty in conducting in-stream measurements during high flow events, most field work was conducted before or after storms. Hence, the model provides a helpful tool to examine the behavior of extreme events.

#### **3.1. Field Data Collection**

Field work comprised a large portion of this research, consisting of regular flow rate measurements and service of two permanently installed *in situ* instruments (Figure 3). A total of 20 site visits for field data collection during 2016 and 2017 were carried out. Two different locations were selected for continuous *in situ* data collection, one upstream and the other downstream from the restored reach. Table III describes the dates and locations where data collection was completed, showing that the transect B was substituted by the cross section C in 2017 (Figure 4).

During each site visit, a hand-held Acoustic Doppler Velocimeter (ADV) (Figure 3) was used to measure flow rates at several stream cross-sections (including those where the two *in situ* instruments were deployed). The ADV used during this study is a FlowTracker2, which has a resolution of 0.0001 m/s and an accuracy of  $\pm 1\%$  for each one-second sample. The instrument

comprises one transmitter and three receivers. The transmitter generates an acoustic signal at a specific frequency, which is reflected by particles in the water and measured by the receivers. The flow velocity is proportional to the acoustic signal frequency change (Doppler shift). The FlowTracker2 carries out 10 individual velocity measurements per second, computing and recording one individual average velocity sample every second during the averaging time (SonTeck, 2016).



**Figure 3.** Field work and instruments.

**TABLE III. DATES AND LOCATION OF DATA COLLECTION**

	Transect A (Downstream 2016 and 2017)	Transect B (Upstream 2016)	Transect C (Upstream 2017)
5/25/2016	x	x	
5/26/2016	x	x	
6/7/2016	x	x	
6/23/2016	x	x	
7/8/2016	x	x	
7/15/2016	x	x	
8/3/2016	x	x	
8/17/2016	x	x	
8/31/2016	x	x	
9/14/2016	x	x	
9/29/2016	x	x	
10/17/2016	x	x	
11/7/2016	x	x	
12/2/2016	x	x	
5/2/2017	x		
5/10/2017	x		x
6/7/2017	x		x
7/6/2017	x		x
7/26/2017	x		x
8/18/2017	x		x

Two portable sondes (EXO2 model built by YSI Incorporated) were deployed and anchored to the stream bed at the main upstream and downstream cross sections (Figure 3). The two sondes were deployed for research on stream ecology measuring temperature, dissolved oxygen, turbidity, pH, fluorescent dissolved organic matter, conductivity, total dissolved solids and hydraulic pressure. These instruments have a differential stainless steel strain gauge transducer that measures hydraulic and vacuum pressure and automatically determine flow depth based on the pressure difference. The instrument accuracy is  $\pm 0.004$  m for shallow flows (up to 10 m deep) and the resolution is 0.001 m (YSI Incorporated, 2014). The sondes provide continuous flow depth with readings every 15 minutes. Later, as described in the Methods and Results sections, the ADV-measured flow depths and discharges were used to derive rating curves, from which continuous discharge estimates were inferred from the sondes' continuous depth readings.

The stream cross sections were divided into 0.5 m segments and corresponding stream panels. Station and depth information was entered into the ADV at each measurement location and then point velocity was measured. Following raw data collection, the instrument's software derived the total discharge, total area, mean depth and mean velocity. The midsection method was used with the ADV to compute the total discharge. In this method, the mean velocity at each measurement location (comprised of one or more measurements in the same vertical) is assumed to represent the mean velocity in the corresponding stream panel. Panels extend horizontally from the midpoint between the previous to the current location, up to the midpoint between the current to the next location. The panel depth corresponds to the flow depth at the measurement location. Equation (1) is used to calculate the total discharge with the midsection method (Turnipseed and Sauer, 2010).

$$Q = \sum_{i=1}^n v_i \left[ \frac{b_{(i+1)} - b_{(i-1)}}{2} \right] d_i \quad (1)$$

where  $Q$  = cross-sectional flow rate ( $\text{m}^3/\text{s}$ ),  $v_i$  = average velocity at measurement location  $i$  ( $\text{m}/\text{s}$ ),  $b_{(i-1)}$  = the previous measurement location along the channel cross-section ( $\text{m}$ ),  $b_{(i+1)}$  = the next measurement location ( $\text{m}$ ) and  $d_i$  = flow depth at measurement location  $i$  ( $\text{m}$ ).

### **3.2. Numerical Model**

The modeling work in this study uses the HEC-RAS (Hydrologic Engineering Center – River Analysis System) model (Hicks and Peacock, 2005) to calculate water surface profiles for steady, gradually-varying flow. HEC-RAS, created by the U.S. Army Corps of Engineers, has become a popular tool in simulating a variety of hydraulic and hydrologic processes including 1D steady flow hydraulics, 1D and 2D unsteady flow hydraulics, quasi unsteady and fully unsteady

flow sediment transport and mobile bed modeling (Brunner, 2016b). The one-dimensional energy equation (2) is the governing equation of HEC-RAS used in the present study (Brunner, 2016a).

$$Z_1 + Y_1 + \frac{a_1 V_1^2}{2g} = Z_2 + Y_2 + \frac{a_2 V_2^2}{2g} + h_e \quad (2)$$

where  $Z_1$  and  $Z_2$  = stream bed elevations (m),  $Y_1$  and  $Y_2$  = flow depths (m),  $V_1$  and  $V_2$  = mean velocities (m/s),  $a_1$  and  $a_2$  = dimensionless velocity head weighting coefficients, computed based on the carrying capacity (conveyance) of the channel and the left and right overbanks (Brunner, 2016a),  $g$  = gravity force ( $m/s^2$ ) and  $h_e$  = energy head loss (m).

The energy head loss (3) between two adjacent transects results from friction (Manning's equation) as well as minor losses due to contraction or expansion (coefficient multiplied by the change in velocity head) (Brunner, 2016a).

$$h_e = LS_f + C \left| \frac{a_1 V_1^2}{2g} + \frac{a_2 V_2^2}{2g} \right| \quad (3)$$

where  $L$  = discharge weighted reach length (m),  $S_f$  = friction slope between two adjacent transects (m/m),  $C$  = expansion or contraction loss coefficient ( $C_{\text{Contraction}} = 0.1$ ;  $C_{\text{Expansion}} = 0.3$ ), that is determined based on the velocity increase (contraction) and velocity decrease (expansion) in the downstream direction (Brunner, 2016b).

The one-dimensional energy equation (2) is solved by HEC-RAS from one transect to the next by iteration using the standard step method, in which computations start at the most downstream cross section and continue in the upstream direction. Discharge, channel geometry and roughness are provided to the model as inputs. The flow depth at the initial cross-section

( $Y_2$ ) is determined based on the provided boundary condition (normal depth in our study). The model assumes a flow depth at the next cross-section in the upstream direction ( $Y_1$ ) based on the previous transect's flow depth. The cross-sectional area, conveyance, velocity head and velocity head coefficient are calculated for transect 1. The friction loss between the two sections is computed and the expansion or contraction loss coefficient determined, and then, the energy head loss (3) is calculated. At this point, the energy equation is solved for transect 1. In the case this equation is not balanced, a new  $Y_1$  value is selected and computations are repeated. Once the energy equation is balanced (agreement within 0.003 m) the computation process moves to the following sub-reach upstream. The described method is repeated step by step until the water surface elevation for all the cross sections of the reach has been calculated (Brunner, 2016a; Davidian, 1984).

HEC-GeoRAS, an extension of ArcGIS, has been used in this research to prepare the geospatial data (i.e., the model transects and elevation data) required by HEC-RAS for subsequent hydraulic analysis. The Digital Terrain Model (DTM) of the pre- and post-restoration stream configurations were provided by WBK Engineering, LLC. The pre-restoration DTM was created by combining site survey and 2-foot interval contour lines obtained from DuPage County. The DTM corresponding to the restored morphology was created based on the designed elevations for the stream channel and floodplain.

As a consequence of the longer channel and greater variety of hydraulic conditions in the restored reach, a larger number of transects and higher transect density was required for the restored stream. In the pre-restored reach 7.2 transects per 100 m were defined. The transect density for the restored reach was defined by sections: the meandering sub-reach required 10.7 transects per 100 m and the two straight unaltered sub-reaches (upstream of the vehicle bridge and downstream of transect A) used 8.37. The intersection between the DTM and model

transects (Figure 4) defines the 3D stream cross-sections used in the model. The same applies in order to define the 3D geometric data corresponding to the river center line, river banks, flow path and bridges required by HEC-RAS. HEC-GeoRAS can also process the water surface and velocity results obtained with HEC-RAS for additional spatial analysis (Ackerman, 2011), such as the flood calculations shown in Figure 13 of the Discussion section.

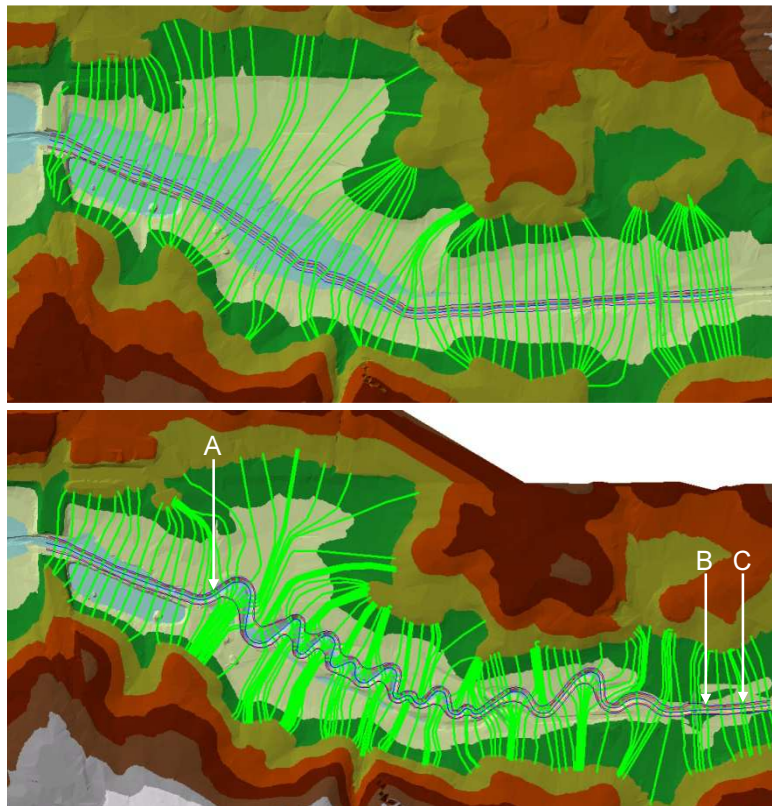


**Figure 4.** (A) Pre-restoration reach GIS layers; (B) Restored reach GIS layers.

HEC-RAS also requires additional information concerning channel and floodplain roughness coefficients for all cross sections as well as detailed definition of structures like bridges, as the initial step in the model preparation.

Based on the low mean flow conditions of approximately 0.4 m<sup>3</sup>/s at Spring Brook, subcritical flow regime has been considered to represent best the stream hydrodynamics. For a subcritical flow regime, HEC-RAS requires defining boundary conditions at the most downstream transect only. This is needed to establish the initial flow depth as described in the standard step method. The boundary condition selected for this work was normal depth, for which the model requires entering an energy slope. Here, we approximate the energy slope to be the same as the average slope of the channel in the proximity of the transect (0.00116 m/m).

The flow simulations in this modeling work were established by prescribing flow rate and letting the software compute water surface elevations using the standard step method. Two different discharge datasets are used in this study, the first one corresponds to 20 field measurements collected with the ADV during the 2016 and 2017 seasons, which is the basis for model calibration as well as subsequent hydraulic analysis. The second dataset corresponds to a return frequency analysis derived from data provided by WBK Engineering (Appendix), which has been used for flood event analysis. The two datasets are included in Table IV.

**TABLE IV. COLLECTED DISCRETE DATA AND FLOW FREQUENCY ANALYSIS RESULTS**

Field data collected during 2016 and 2017						Return frequency analysis	
Date	H max (m)	Q (m <sup>3</sup> /s)	Date	H max (m)	Q (m <sup>3</sup> /s)	Return period (years)	Q (m <sup>3</sup> /s)
5/25/16	0.29	0.45	9/29/16	0.28	0.34	1	5.45
5/26/16	0.47	1.09	10/17/16	0.30	0.26	2	10.81
6/7/16	0.29	0.39	11/7/16	0.23	0.29	5	16.22
6/23/16	0.30	0.33	12/2/16	0.27	0.29	10	20.83
7/8/16	0.30	0.40	5/2/17	0.70	2.53	25	28.05
7/15/16	0.23	0.21	5/10/17	0.37	0.72	50	34.59
8/3/16	0.28	0.30	6/7/17	0.23	0.24	100	42.26
8/17/16	0.26	0.21	7/6/17	0.26	0.19		
8/31/16	0.30	0.41	7/26/17	0.34	0.50		
9/14/16	0.26	0.22	8/18/17	0.20	0.17		

The HEC-RAS model returns a number of hydraulic variables of interest at each cross section, including the flow velocity and depth, shear stress, and stream power, which are discussed in the Discussion section.

### **3.3. Rating Curves: Model Calibration**

A fundamental step of this research involves the derivation of stage-discharge relationships or “rating curves”. We construct rating curves at the upstream and downstream transects where the sondes are located based primarily on the interdependent stage and discharge field data collected from the ADV (Domeneghetti et al., 2010). The paired H-Q data during 2016 and 2017 were used to derive graphical curves and mathematical expressions that relate the two variables. The overall objective for deriving these empirical relationships is to serve as means for obtaining continuous flow rate records from continuous stage measurements (from permanent instrument readings). However, the process leading to the final procurement of these rating curves is essentially the HEC-RAS model calibration.

The calibration process started once the HEC-RAS model was completely built (e.g. the stream geometry and boundary and initial conditions were defined). The model was run using the discharge values collected in the field (Table IV) as initial conditions for a variety of stream channel and floodplain roughness values (Manning’s n number) in 0.001 increments, from 0.035 to 0.055, for the channel and 0.01 increments, from 0.10 to 0.20, for the floodplain. For every run, the software provided a stage-discharge relationship for every cross-section. Then, the rating curves corresponding to the two study transects were selected from the model and compared with the H-Q relationships obtained from field data collection (ADV and sondes). We

selected the Manning's n number that best matched the model rating curves with the observed rating curves for the two study transects.

As part of the calibration process, the post-restoration stream channel was divided in two different sections. The first one corresponds to the unaltered region upstream from the vehicle bridge. The second sub-reach corresponds to the region downstream of the vehicle bridge that was altered during the meander restoration. These two sections have different channel geometries and roughness characteristics and different Manning's n numbers were assigned to each section.

No roughness data related to the pre-restored stream channel is available. However, the sub-reach upstream from the vehicle bridge in the post-restoration situation is identical to the pre-restored stream channel (e.g. stream alignment and bed material). Hence, the resulting roughness value from the calibration process for the former case was assigned to the latter.

### **3.3.1. Downstream Rating Curves**

Figure 5 shows the rating curves (Q versus H) for multiple field observations (by both the ADV and the sonde), for the HEC-RAS model, and for Manning's equation (4) at the downstream studied cross section at Spring Brook.

The "Velocimeter" curve plots the flow depth and flow rate derived from 20 ADV field measurements (Table IV), which results in a best-fit, power-law relationship of  $H = 0.4439Q^{0.3975}$ . The "Sonde" curve uses the flow rates observed in the field from the ADV and relates that to the simultaneous flow depth values that were observed from the sonde, giving a stage-discharge

relationship that closely approximates the “Velocimeter” curve ( $H = 0.4364Q^{0.37}$ ). The “HEC-RAS Model” curve is also very consistent with the two previous H-Q relationships ( $H = 0.4349Q^{0.4101}$ ), suggesting the model, once calibrated, provides a suitable characterization of the studied cross section. Finally, we compared the observed/modeled rating curves to the theoretical rating curve obtained from Manning’s equation (using a channel slope of 0.0017 m/m, derived from the DTM).

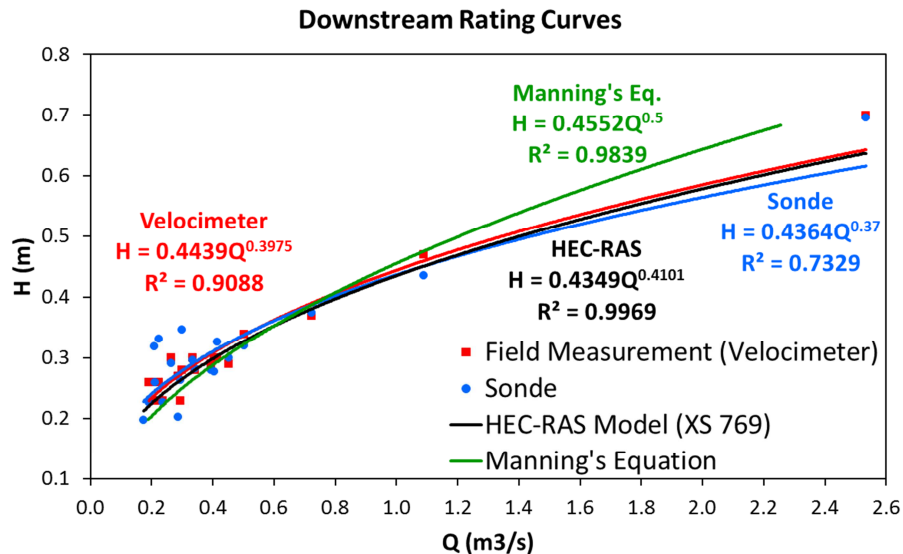


**Figure 5.** Downstream rating curves used for model calibration and estimation of flow rates based on direct measurements of flow depth.

A Manning’s  $n$  number of 0.045 (which according to Brunner (2016a) is characteristic of clean and winding stream channels with some pools, shoals, weeds and stones) was selected for the restored channel (sub-reach downstream from the vehicle bridge) as the final result from the calibration process. Regarding the floodplain, the best fit corresponds to a Manning’s  $n$  number of 0.16 that corresponds to dense brush, in summer (Brunner, 2016a). Table V shows the calibrated Manning’s  $n$  numbers.

**TABLE V. MANNING'S ROUGHNESS NUMBER OPTIMIZED FOR THE MODELING WORK**

	Pre-restored stream	Restored stream	
		Sub-reach upstream of the vehicle bridge	Sub-reach downstream of the vehicle bridge
Channel	0.040	0.040	0.045
Floodplain	0.16	0.16	0.16

Manning's equation (4) is a widely used relationship to predict stream discharge (Q) from hydraulic variables (Sefick et al. 2015). In the following analysis, we will demonstrate theoretical arguments as to why we find the empirically-derived powers of ~0.37-0.41 in the resulting H-Q relationships. We begin with Manning's equation,

$$Q = \frac{1}{n}AR^{2/3}S^{1/2} \quad (4)$$

where n = Manning's roughness coefficient, A = Cross-sectional area (m<sup>2</sup>), R = Hydraulic Radius (m) and S = Channel bottom slope (m/m). In the channel dimensional analysis we assume that the incised pre-restoration channel resembles a quasi-rectangular section and that the restored channel is more similar to a trapezoidal section.

#### **Rectangular section (pre-restored channel):**

In a rectangular section (Figure 6) the cross-sectional area is defined as the width times the depth (A = wH). The hydraulic radius (R) is determined by the cross sectional area (A) divided by the wetted perimeter (P). Assuming that the channel is much wider than it is deep (w>>H), the 2H term (representing the channel walls) in the wetted perimeter is negligible in comparison to the channel width. Thus, we can obtain that R≈H, as follows:

$$R = \frac{A}{P} = \frac{wH}{w + 2H} \approx \frac{wH}{w} = H$$

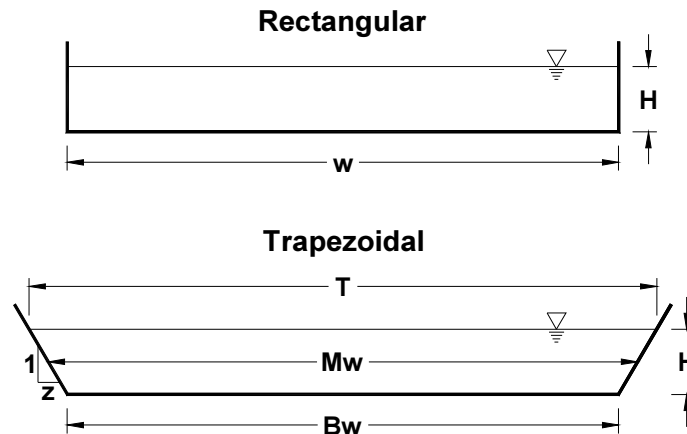


**Figure 6.** Rectangular and trapezoidal open channel geometry.

Substituting  $A$  and  $R$  into Manning's equation and simplifying, we can obtain:

$$Q = \left( \frac{S^{1/2}}{n} \right) (wH \cdot H^{2/3}) = \left( w \frac{S^{1/2}}{n} \right) (H^{5/3})$$

According to the previous expression, we can determine that  $Q$  is proportional to  $H^{5/3}$  ( $Q \propto H^{5/3}$ ).

Rearranging, we obtain that:

$$H \propto Q^{3/5} = Q^{0.6}$$

#### **Trapezoidal section (restored channel):**

In a trapezoidal channel (Figure 6), the cross-sectional area ( $A$ ) can be calculated as the mean channel width ( $M_w$ ) times the flow depth ( $H$ ). If the channel wall slopes are  $z:1$  (horizontal to vertical increment ratio), the average channel width can be determined as:

$$M_w = T - zH$$

where, T is the top width, which is proportional to H. Then we have:

$$M_w = \alpha H - zH = \beta H$$

Consequently, the cross-sectional area is:

$$A = \beta H \cdot H = \beta H^2$$

The wetted perimeter (P) in a trapezoidal channel is defined as the bottom width plus the two wall length.

$$P = B_w + 2H\sqrt{1 + z^2}$$

The bottom width can be determined as:

$$B_w = T - 2zH$$

Then, substituting and simplifying, the wetted perimeter can be expressed as follows:

$$P = (T - 2zH) + 2H\sqrt{1 + z^2} = (\alpha H - 2zH) + 2H\sqrt{1 + z^2} = \gamma H$$

Substituting A and P in the hydraulic radius equation we have that R is proportional to H:

$$R = \frac{A}{P} = \frac{\beta H^2}{\gamma H} = \delta H$$

Finally, substituting all the variables into Manning's equation we obtain:

$$Q = \frac{1}{n} AR^{2/3} S^{1/2} = \left( \frac{S^{1/2}}{n} \right) (\beta H^2 \cdot (\delta H)^{2/3}) = \left( \beta \cdot \delta^{2/3} \cdot \frac{S^{1/2}}{n} \right) (H^{8/3})$$

Then, we can state that Q is proportional to  $H^{8/3}$  ( $Q \propto H^{8/3}$ ). Rearranging, we obtain that:

$$H \propto Q^{3/8} = Q^{0.375}$$

This expression agrees with the power relationships of ~0.37-0.41 from the observed and model rating curves. Applying the unapproximated Manning's equation (4) to the stream cross-section at the downstream sonde location (derived from the ADV) results in a best fit power of approximately 0.5, which is ~25% higher than the powers obtained from the observed/modeled rating curves.

If we compare the two channels assuming that they have the same bottom width, a specific discharge increment would cause a higher flow depth increment in the case of the rectangular channel, as Figure 7 shows.

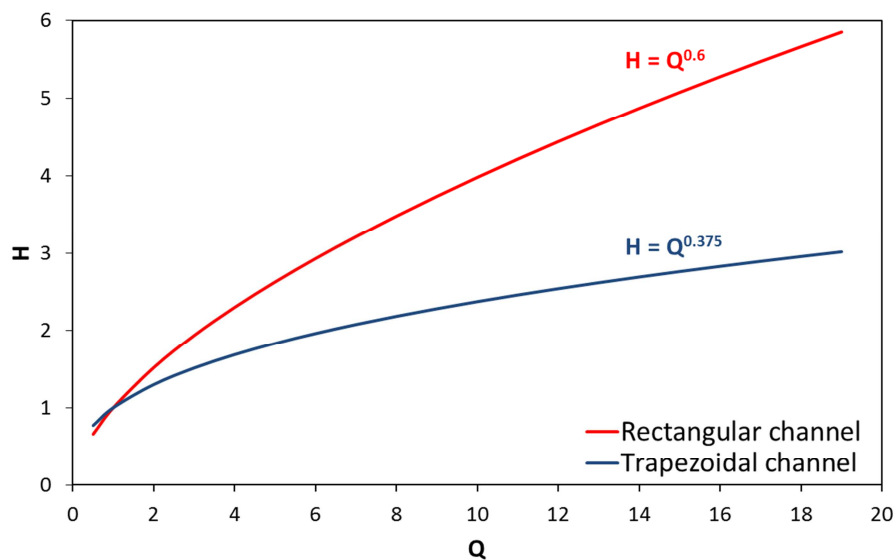


**Figure 7.** Stage-discharge relationship for an ideal rectangular and trapezoidal stream channel.

### 3.3.2. Upstream Rating Curves

Figure 8 displays the rating curves for field observations and the HEC-RAS model at the cross section near the upstream sonde at Spring Brook. The field observations of H versus Q exhibited more scatter than at the downstream site during the 2016 field work season, possibly due to sediment deposition and stream bed settling/compaction during depth readings. Consequently, the upstream studied transect was relocated 48 m upstream from the original site for the 2017 season (Table III and Figure 4). The data collected during the 2017 season at the upstream location appear to be more consistent.

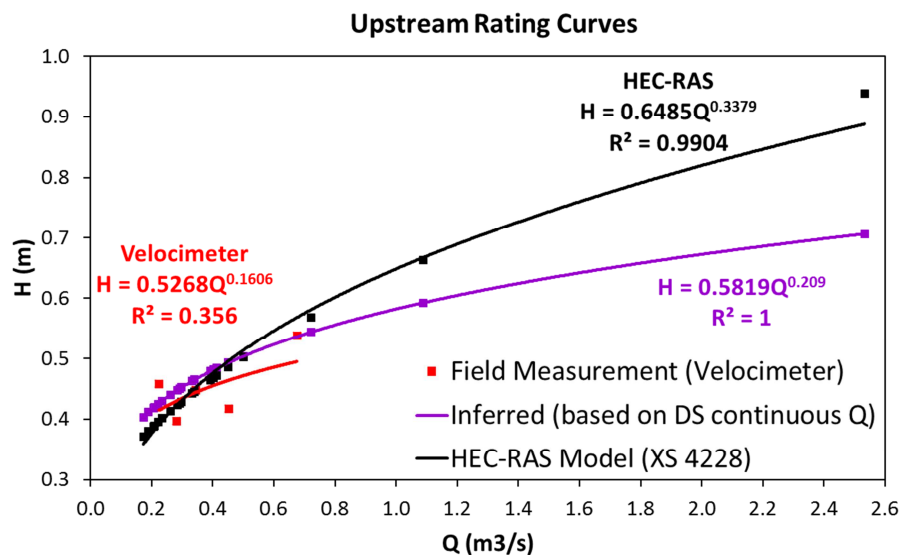


**Figure 8.** Upstream rating curves used for model calibration.

The “Velocimeter” curve on Figure 8 plots the limited series of flow depth and flow rate data manually collected in the field with the ADV during 2017 only. These data also exhibit some degree of scatter. The “Inferred” rating curve was built based on the continuous flow rates

derived from the downstream sonde rating curve and the continuous flow depths observed from the upstream sonde during the 2017 season, considering a one-hour delay due to the water travel time between the two locations. This “Inferred” curve was constructed based on the assumption that the stream discharge must be roughly equal at the upstream and downstream sites, since little stream flow is expected to be lost or gained from groundwater infiltration or resupply, respectively, over the relatively short reach of the stream. Furthermore, the consistency between the observed and modeled rating curves at the downstream site gives a higher degree of confidence in the continuous discharge values derived at this location. Thus, the “Inferred” H-Q relationship ( $H = 0.5819Q^{0.209}$ ) was then used to determine the flow depths at the upstream transect for the 20 ADV-observed flow rates (Table IV). The “HEC-RAS Model” curve relates the 20 simulated flow depths at the upstream cross section obtained from the 20 ADV-observed flow rates applied as initial conditions in the model.

Due to the limited amount of field data collected with the ADV in 2017 at the new upstream site, as well as the limited range of flow regimes observed within these data, the stage-discharge relationship results are not as robust as those at the downstream site. Furthermore, the upstream site is characterized by a larger amount of aquatic vegetation, which may cause roughness values to vary with flow conditions, and therefore preclude straightforward derivations of stage-discharge relationships.

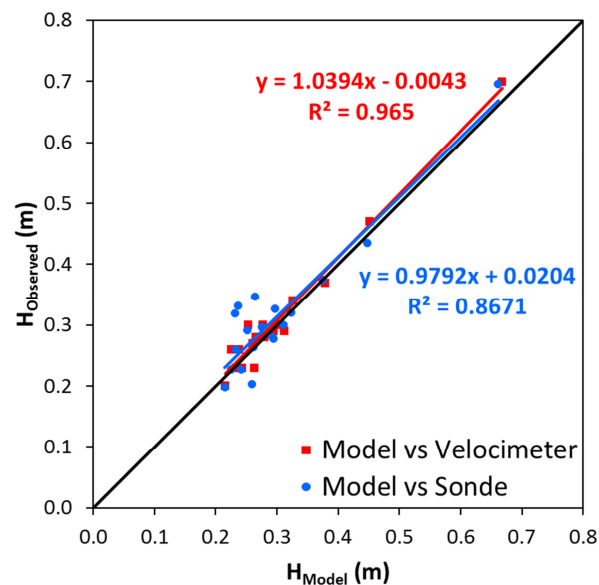
A Manning’s n number of 0.040 (which according to Brunner (2016a) is characteristic of clean and winding stream channels with some pools and shoals) was selected for the unaltered sub-reach (upstream from the vehicle bridge) of the current stream configuration as the final HEC-RAS model calibration result. Regarding the floodplain, the Manning’s n value obtained for this case is also 0.16. These roughness values are also applied to the pre-restoration model. Table V lists all the Manning’s n values optimized for this model.

## 4. RESULTS

### 4.1. Model Validation

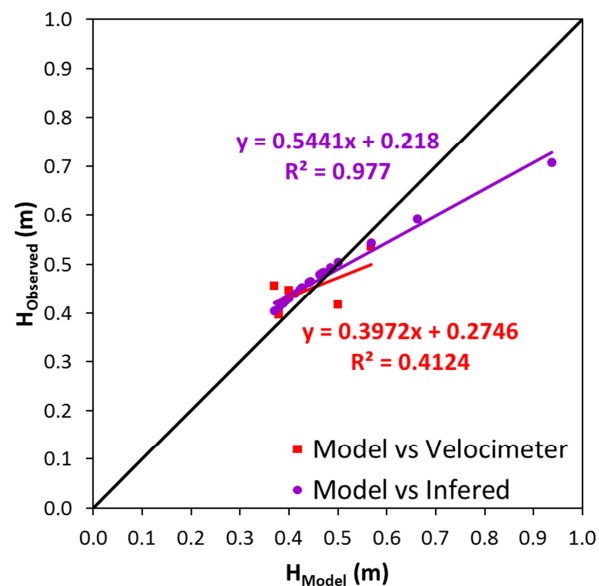
The model validation has been carried out by the comparison between the flow depth values resulting from the HEC-RAS model simulation and the corresponding flow depths measured in the field (by the ADV and the sondes). In the upstream case, the model results are also compared to the “Inferred” relationship.

Figure 9 shows the validation outcomes for the downstream study site. The model presents a high degree of agreement with both ADV and sonde H measurements. This location has a good behavior and the model captures the flow variations very accurately. The DTM resolves the channel very well at the downstream site and the optimal roughness values have been selected.



**Figure 9.** Model validation for the downstream data collection site.

For the upstream site, Figure 10 shows the obtained validation results, which are not as robust as in the previous case. Only 5 field H-Q measurements with ADV were completed at transect C, as a consequence of the relocation of the study site in 2017 and more reduced field season. The variability of hydraulic conditions observed during those 5 field visits was also very limited as compared with the downstream site data. Looking at the model versus “Inferred” line, further analysis in order to determine a more accurate flow travel time between the upstream and downstream sites for different flow conditions would have possibly improved the consistency. Finally, another possible reason for the lower agreement at this site can be the DTM capability to represent the channel characteristics at this upstream region.



**Figure 10.** Model validation for the upstream data collection site.

#### **4.2. Continuous flow depth and flow rate readings**

The two portable sondes installed at the upstream and downstream transects provide continuous flow depth measurements from the instruments' pressure sensors every 15 minutes.

Figure 11 displays the continuous flow depth data collected by the two portable sondes installed at the upstream and downstream transects compared to the co-located depth measurements from the ADV, showing excellent agreement between the two for transects A and C. Less consistency can be observed in the case of transect B, which supports the relocation of the upstream site to transect C.

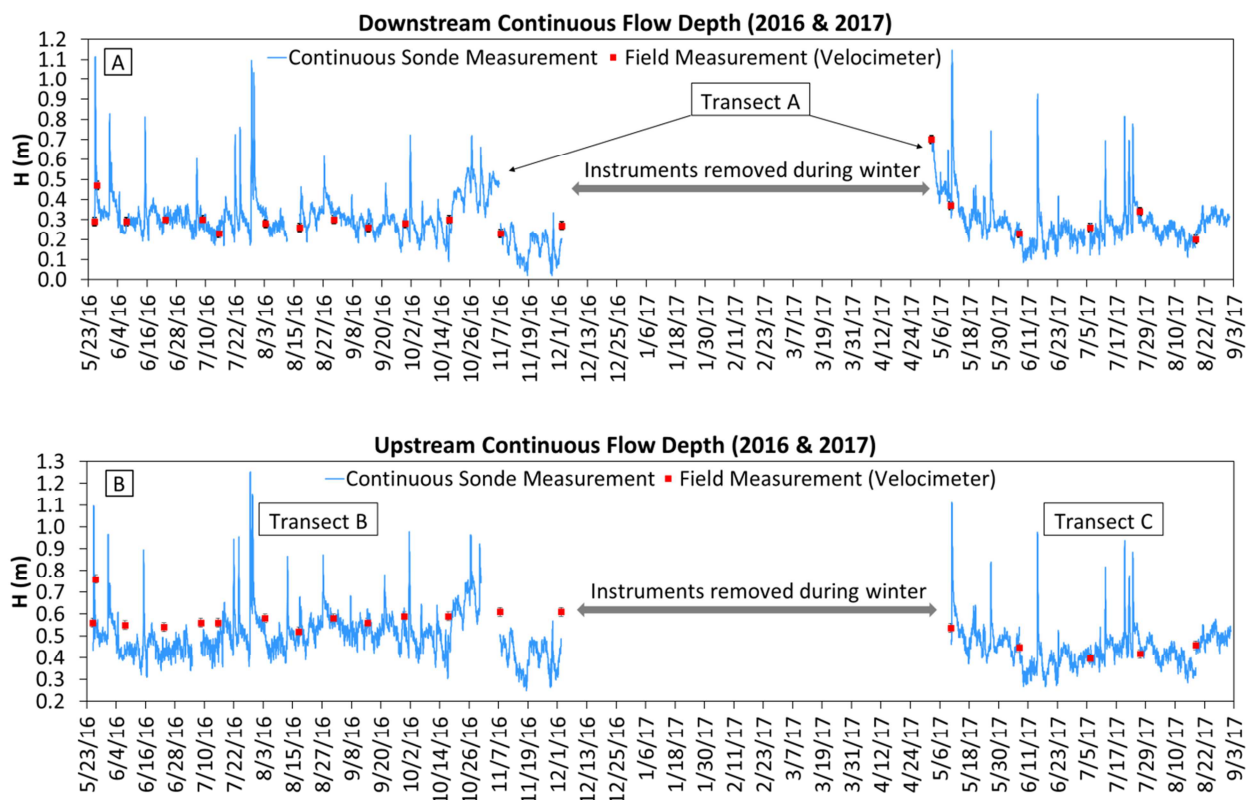


**Figure 11.** Continuous flow depth for the two data collection sites.

Panel A shows the data corresponding to both the 2016 and 2017 field work seasons for the downstream site. Multiple peaks can be observed, with a maximum water depth of 1.14 m at the beginning of May 2017. Panel B shows the upstream data for the 2016 and 2017 field work seasons. An offset of approximately 0.2 m between depth data from transect B and transect C

has been determined. Some daily fluctuations can be observed in the base flows as a consequence of the effluent released from the wastewater treatment plant located 1.2 km upstream of the Spring Brook study site.

The continuous flow depth from the sondes (Figure 11) and the derived stage-discharge relationships were combined to infer continuous flow rates (Figure 12).

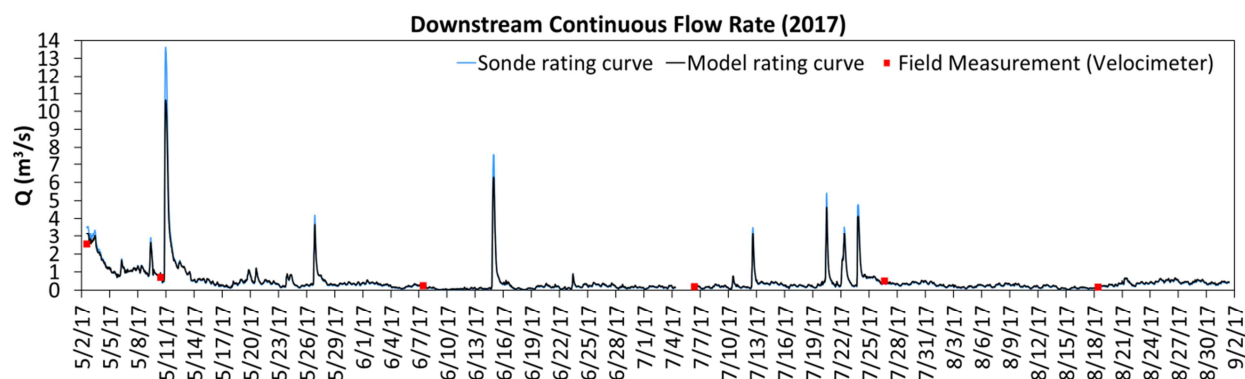


**Figure 12.** Continuous flow rate determined at the downstream data collection site.

Figure 12 shows continuous flow rates for the 2017 season derived from applying the continuous flow depth data from the downstream sonde to both “HEC-RAS Model” rating curve and “Sonde” rating curve, constructed for the same transect. ADV-measured flow rates are also included in Figure 12 which demonstrate an excellent agreement with the continuous measurements, despite the tendency to sample only base flow conditions. The two continuous flow rate curves are almost identical, with the model slightly under-predicting the discharge during high-flow events. The consistency between the continuous modeled/observed flow rates in Figure 12 likely results from the consistency between the rating curves shown in Figure 5, resulting from the calibration process. This gives a reasonable degree of confidence in inferring

the magnitudes of high flow events, which are later used to assess the degree of connectivity between the stream channel and the flood plain during storms in the Discussion section.

## 5. DISCUSSION

A major hydraulic objective of the restoration project was to achieve lateral connectivity between the stream channel and the flood plain. Lateral connectivity implies the hydraulic transfer of energy, matter and organisms between a stream and their adjacent flood plain that occur during moderately recurrent stream flow events that inundate the floodplain (Booth et al., 2001; Ickes et al., 2005) rather than only during the highest flow events. Some benefits of reestablishing lateral connection include erosion reduction, improved floodplain ecological function and species richness (Booth et al., 2001; Simon et al., 2011; Roni, P. and Beechie, T. 2013).

The restoration project constructed meanders and depressed connection channels and restored wetlands in order to accomplish this objective (see Figure 13B).

Figure 13 shows the results obtained from the 2D modeling using HEC-GeoRAS and HEC-RAS. Five different flow rate scenarios were considered: 0.4 m<sup>3</sup>/s (average base flow rate), 2.5 m<sup>3</sup>/s (highest flow rate manually measured in the field with the ADV), 5.4 m<sup>3</sup>/s (equivalent to 1-year return period), 20.8 m<sup>3</sup>/s (equivalent to 10-yr return period) and 42.3 m<sup>3</sup>/s (equivalent to 100-yr return period).

Panels A and B show that for base flow rates, limited inundation of the adjacent floodplain occurs only in the restored case (as the restored wetland pools start to fill up). For discharges of 2.5 m<sup>3</sup>/s, panels C and D again show continuous hydraulic interaction between stream channel and floodplain for the restored reach case only (as all adjacent depressions become hydraulically connected to the channel and wetland pools become flooded), while in the pre-restored stream, the flow is completely isolated to the main channel.

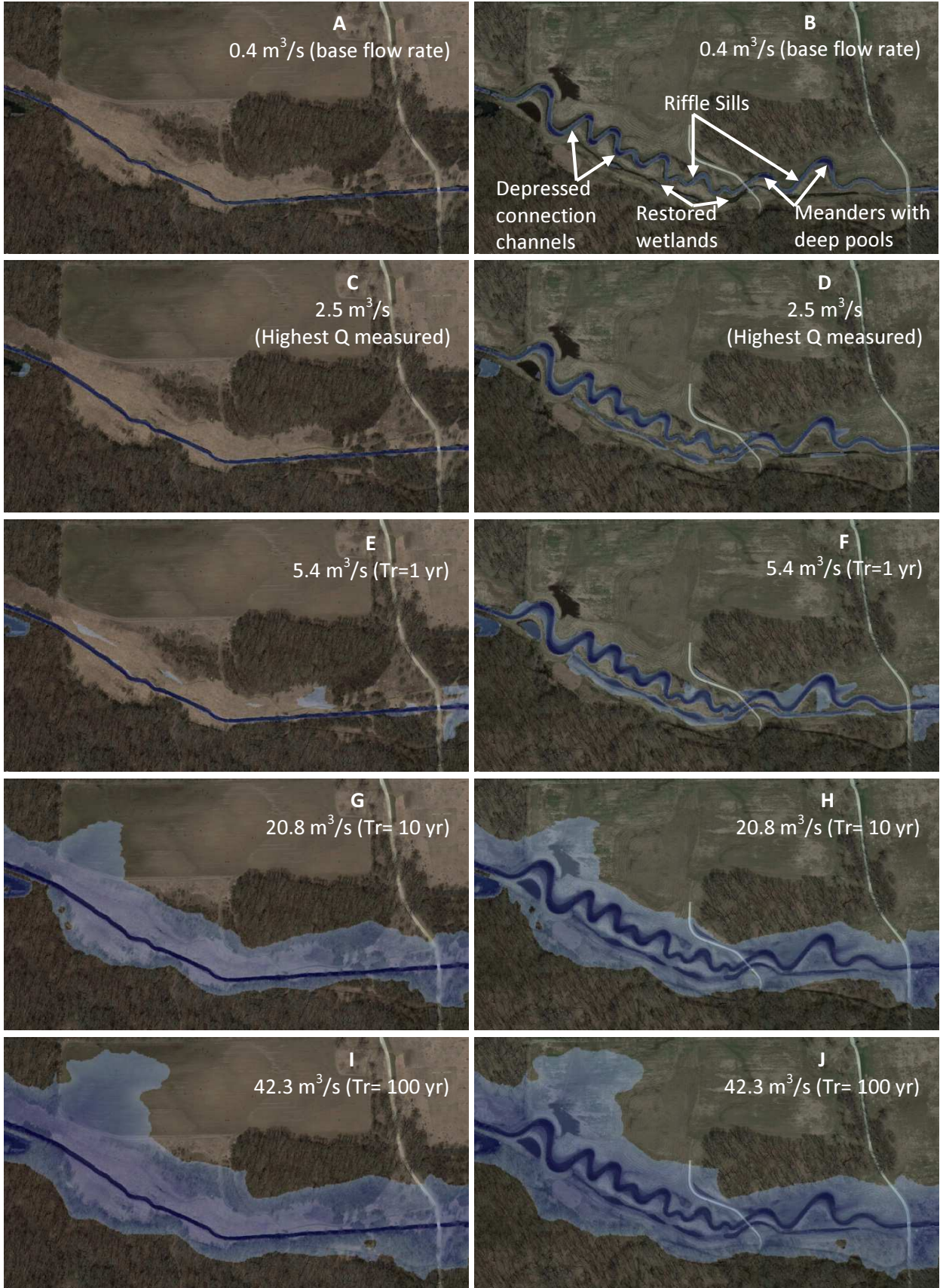


**Figure 13.** Flood maps for the pre-restored and the restored stream configurations. Aerial imagery obtained from Google Earth.

For discharges of 5.4 m<sup>3</sup>/s (corresponding to the 1-year flow event), some depressions start to fill up in the pre-restoration case (panel E) as the water surface elevation simulated by HEC-RAS is higher than the terrain, and panel F starts to show a flooded floodplain, however the transition for the restored reach has been gradual up to this stage. Panels E and F also show the backup effect caused by the vehicle bridges. Finally, panels G to J display complete and extensive floodplain inundation for discharges of 20.8 and 42.3 m<sup>3</sup>/s that correspond to the 10 and 100-year floods, respectively.

A stream restoration project has the potential for substantial modification of many important hydraulic variables. Because those modifications can pose relevant consequences in the stream hydrodynamics and habitat, it's worth analyzing the degree of alteration in terms of the new range in conditions and their change in distribution. Here we pay special attention to the flow depth, flow velocity, shear stress and stream power, since they represent fundamental hydraulic variables of interest.

The shear stress (N/m<sup>2</sup>) (5) is a force applied in the flow direction and parallel to the plane in which friction force resists the former when in equilibrium (Brunner, 2016a).

$$\tau_0 = \gamma RS \quad (5)$$

where,  $\gamma$  = specific weight of water (N/m<sup>3</sup>), R = hydraulic radius (m), S = slope (m/m). The shear stress of a flow is compared with the critical shear stress of a specific sediment size as the limit condition for incipient motion and related channel instability (Brunner, 2016a; Mays, 2010). The

dimensionless shear stress can be obtained from the Shields diagram for different particle sizes and then, the critical shear stress is computed using equation (6)

$$\tau_c = \tau_* (\gamma_s / \gamma - 1) \gamma D_s \quad (6)$$

where  $\tau_*$  = dimensionless shear stress,  $\gamma_s$  = specific weight of particle ( $\text{N/m}^3$ );  $D_s$  = particle diameter (m). The Shield diagram has been rearranged by other authors to directly obtain critical shear stress from particle size (Mays, 2010). Transport occurs when  $\tau_0 > \tau_*$ .

Stream power is a measure of energy that potentially can move sediments, a quantity that is frequently used for stream stability analysis (Makaske, 2001). The specific stream power ( $\text{N/m}\cdot\text{s}$  or  $\text{W/m}^2$ ) (7) represents the rate at which potential energy is applied to a stream bed per unit area (Knighton, 1999):

$$\omega = \frac{\rho g Q s}{w} = \tau_0 v \quad (7)$$

where  $\rho$  = density of water ( $\text{kg/m}^3$ ),  $g$  = gravity force ( $\text{m/s}^2$ ),  $Q$  = flow rate ( $\text{m}^3/\text{s}$ ),  $s$  = energy slope ( $\text{m/m}$ )  $\approx$  channel bed slope,  $w$  = channel width (m),  $\tau_0$  = mean boundary shear stress ( $\text{N/m}^2$ ) and  $v$  = average flow velocity ( $\text{m/s}$ ). Low specific stream power values ( $< 60 \text{ N/m}\cdot\text{s}$ ) are typical from stable streams (Makaske, 2001).

Figure 14 shows the range of hydraulic conditions associated with all discharge values observed during field work at all modeled transects in the pre-restored and restored stream. As a consequence of the restoration project, the stream now contains deep pools around many of the meanders. The restored reach holds a larger depth range compared to the pre-restored conditions, with the major difference being due to the deep meander pools. These new deep pools have also facilitated a higher frequency of occurrence of very slow velocities. Additionally,

some regions with high velocities in the pre-restored case have disappeared as a consequence of the re-meandering. Various riffles have been added to the restored stream bed, which increase velocity in their downstream regions, but unfortunately, these structures are not captured by the terrain model.

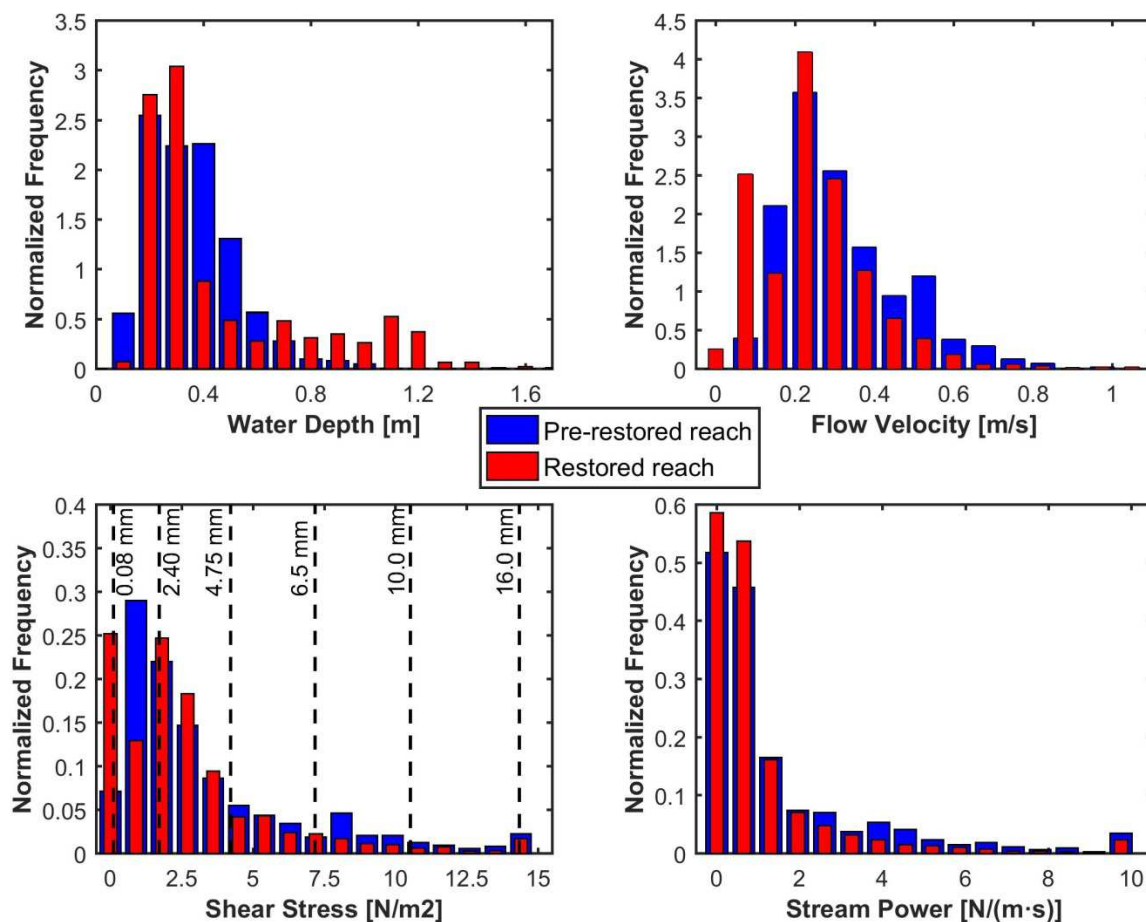


**Figure 14.** Probability distribution for hydraulic variables before and after stream restoration. The analyzed variables are flow depth, flow velocity, shear stress and stream power. The last bins of the shear stress and stream power plots contain all the observations greater than 15 N/m<sup>2</sup> and 10 N/(m·s), respectively.

The shear stress plot on Figure 14 shows that the pre-restored and restored conditions are very similar. In general, the shear stress has been slightly reduced for the restored case as a

consequence of the deep pools. This plot also shows the incipient shear stress thresholds for various particle sizes. Sand (0.08 mm) and very fine gravel (2.4 mm) are subject to be continuously transported since their reduced critical shear stress limits are within the range of the most probable shear stress values of the channel. As we consider bigger particle diameters, the probability for them to be moved is lower. In the case of medium (10 mm) and coarse gravel (16 mm), only infrequent high flow events would cause the transport of these materials (Buffington and Montgomery, 1999). The stream power plot does not show much difference between the two cases either. However, there is a small frequency increase of lower values and a small frequency reduction of higher values of stream power, possibly derived from a stream bed slope reduction and channel widening as part of the restoration project. The highest modeled value of stream power for flow rates up to 2.5 m<sup>3</sup>/s is approximately 55 N·m<sup>-1</sup>·s<sup>-1</sup>, which is below the 60 N·m<sup>-1</sup>·s<sup>-1</sup> threshold for stream stability problems.

Habitat diversity depends on the stream physical morphology (i.e. bends, sequence of riffles and pools, spatial variations of flow velocity, variety of bottom substrates, etc.). Many studies focus on habitat diversity to evaluate stream health (Cushing and Allan, 2001). The range and distribution of physical conditions of the stream before and after restoration has been analyzed primarily through two variables, flow depth and flow velocity, extracted from the model results. The co-located depth and velocity data required for this analysis was obtained based on the 20 discrete discharge values observed in the field for all of the cross sections used to define the model geometry of the two stream configurations.

Figure 15 shows a scatter plot of the co-located depth and velocity data as well as the univariate and joint probability distributions. The joint probability distribution for the pre-restored case clearly indicates one homogeneous region of higher frequency of occurrence for the co-

located depths and velocities, representing channelized base-flow conditions. This region spans a velocity range of 0.05 to 0.62 m/s and flow depth values between 0.1 and 0.6 m.

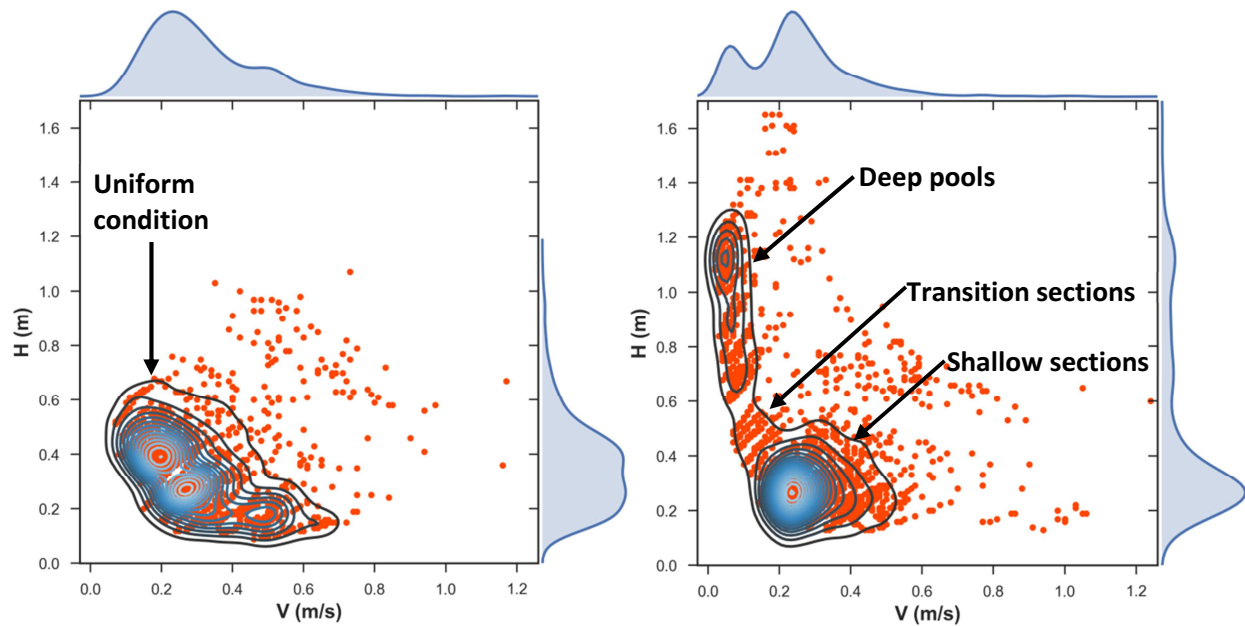


**Figure 15:** Joint probability distribution of water depth and flow velocity for the pre-restored (A) and the restored (B) stream configurations. The plot also shows marginal plots for the independent probability distribution of each variable on the top and right edges.

In the case of the restored configuration, the joint probability distribution plot shows heterogeneity by the clear indication of two different regions with higher frequency of occurrence. The principal region corresponds to intermediate flow velocities that occur in shallow sections of the meandering reach, for which the higher probability of occurrence corresponds to velocity values ranging between 0.15 and 0.45 m/s and depth values from 0.1 to 0.45 m. The secondary region is characterized by very low flow velocity (minimum values close to 0 m/s) and a better distributed range of flow depths with an important representation of deeper sections corresponding to deep pools at the meander bends (more frequent values up to 1.25 m). These

two regions have a narrower aspect as opposed to the pre-restored layout, caused by the reduction of flow velocities achieved by the meandering restoration.

The addition of the second region and transition sections (as shown in Figure 15) to the restored plot is clearly influenced by the deep pools and evidence of more diversified physical stream conditions in the restored configuration.

A well-established method for habitat analysis is based on habitat suitability indices. Curves that provide species preferences for diverse physical conditions at different stages of their life cycle are applied to models that simulate habitats. The geographical analysis of habitats that meet specific species preferences or the evaluation of environmental changes effects in species populations are examples of these models' capabilities (Hickey et al., 2015; Sanz-Ronda et al., 2014).

Invertebrates show that the most important parameter related to their preferred habitat conditions is flow velocity, for which studies have found wide ranges from 0.15 to 1.1 m/s. Typical values for flow depth are between 0.08 and 0.3 m (Gore, 1985). Freshwater mussels preferred habitat conditions are still insufficiently known. However, in general the majority of species find good conditions in streams with flows less than 1 m deep, well oxygenated water and stable substrate containing a combination of sand, gravel and some silt (Machtinger, 2007). Pearl mussels (*Margaritifera margaritifera*) is an endangered fresh water mussel species that can be found in northeastern North America and presents optimum water depth of 0.3 to 0.4 m and preferred flow velocity of 0.25 to 0.75 m/s (Hastie et al., 2000). In the case of fish, different species present very heterogeneous habitat preferences and frequently many of these need access to different kinds of habitats during their life cycle (Waal et al., 1998). The green sunfish (*Lepomis cyanellus*) is indigenous of the Great Lakes area and has a preference for stream

pools. Its habitat suitability curves suggest that adults and juveniles prefer flow velocities lower than 0.1 m/s. Spawning occurs at depths of 0.04 to 0.35 m and embryos preferred flow velocity is lower than 0.1 m/s, with a maximum tolerable value of 0.15 m/s (Stuber et al., 1982).

Figure 16 shows the suitability of Spring Brook's physical conditions for invertebrates, pearl mussels and green sunfish for the pre-restored and restored streams by superimposing the habitat preference of these species and group of species over a scatter plot of the co-located depth and velocity data obtained from the HEC-RAS model for all the transects and the 20 discrete flow data collected in the field. Adult and juvenile green sunfish's preference for stream pools has been quantitatively resolved by considering pools as regions deeper than 0.4 m.

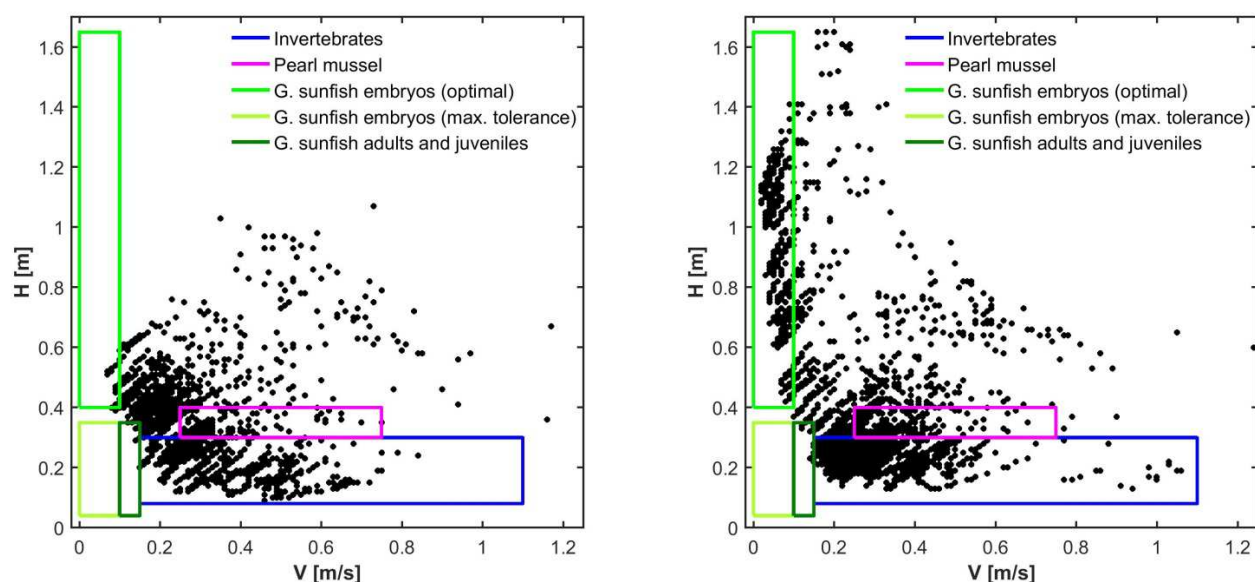


**Figure 16:** Comparison of preferred ranges of flow depth and velocity for invertebrates, pearl mussels and green sunfish with Spring Brook's depth and velocity conditions (before and after restoration).

We observe in Figure 16 that the invertebrate wide range of flow velocity and flow depth preferences are met by both stream cases, meaning that invertebrates would likely find

favorable conditions in the two scenarios. We considered a group of invertebrate species, however, individual cases would probably show different results. Pearl mussels would also find suitable water velocity and depth at Spring Brook in the two configurations; however, further analysis of additional variables should be done in order to determine if this endangered species would actually thrive at Spring Brook. In the case of the green sunfish, only the restored reach would provide a wide range of suitable flow depth and flow velocity conditions for adults and juveniles as a consequence of the addition of deep pools to the restored reach. However, optimal flow velocity conditions for embryos wouldn't be met by any of the two stream configurations. The green sunfish embryos' maximum range of flow velocity tolerance (up to 0.15 m/s) is also included in Figure 16, showing that very limited agreement between the provided and required velocity conditions is met for both before and after stream restoration.

Hence, diversity is fundamental, meaning that the proper combination of flow depth, flow velocities and substrate types is essential to providing suitable food production, spawning-incubation, and cover areas, characteristic of productive stream habitats (Gore, 1985).

## 6. CONCLUSIONS

The extensive modeling work conducted in this research for the pre-restored and the restored stream configurations at Spring Brook, together with the subsequent hydraulic analysis, both supported by comprehensive field data collection, has uncovered many hydraulic differences and improvements afforded by the stream restoration project.

We used the model to extend the spatio-temporal variability of flow conditions within the complete reach and also explore the results for extreme flow conditions that we were not able to measure in the field. We simulated the hydraulic conditions and obtained water surface profiles for all the flow rates manually measured in the field and also some larger return period discharges. Combining the HEC-RAS and the HEC-GeoRAS models we were able to obtain 2D flood results and found that the restored reach has improved the hydraulic connection between the stream channel and the floodplain by allowing a continuous increase of surface water cover on the flood plain for base flow rates and higher. In contrast, the pre-restored stream requires much higher discharge values for the same purpose.

The HEC-RAS model also provided channel flow velocity for every defined cross-section as well as many other variables such as shear stress and stream power. The subsequent analysis of these variables exposed that the meandering restoration achieved a better distributed range of flow depth that includes deep pools and riffles, providing heterogeneity in contrast to the uniform geometry of the pre-restored reach. A small reduction of high flow velocities has been achieved by the meandering and construction of deep pools. The unique combination of flow depths and velocities for the restored stream provides a more diverse range of physical conditions as the basis for new diversified habitats and species richness improvement. Conversely, the pre-restored reach only provided very homogeneous physical

conditions. The model results for shear stress and stream power show a small reduction of the two variables for the 20 simulated discharge values. Additionally, the obtained stream power values indicate low risk of instability for flow rates up to  $2.5 \text{ m}^3/\text{s}$ , suggesting that the restored reach will likely maintain its configuration for several years.

One limitation encountered during the modeling process consists of the fact that the terrain model does not define some in-stream features like the riffle sills, which play a non-negligible effect on the stream hydraulics. This limitation may be overcome by obtaining high-resolution, site-specific terrain elevation data (from methods like aerial LIDAR or structure-from-motion) and applying a 2D, grid-based model. An additional contribution of this research is the derivation of accurate stage-discharge relationships for the restored stream, which can aid many new studies at the site. Overall, the modeling work and additional analysis have provided information that allows concluding that, in hydraulic terms, the stream restoration appears to have been successful.

## REFERENCES

- Ackerman, C. T. (2011). *HEC-GeoRAS: GIS Tools for Support of HEC-RAS using ArcGIS, User Manual*. Davis, CA: US Army Corps of Engineers.
- ASCE River Restoration Subcommittee on Urban Stream Restoration. (2003). *Journal of Hydraulic Engineering*, 129(7), 491-493.
- Booth, D.B. & Fischenich, C.J. (2015). A channel evolution model to guide sustainable urban stream restoration. *Area*, 47(4), 408–421.
- Booth, D. B., Karr, J. R., Schauman, S., Konrad, C. P., Morley, S.A., Larson, M. G., Henshaw, P. C., Nelson, E. J., & Burges, S. J. (2001). *Urban stream rehabilitation in the Pacific Northwest*. University of Washington.
- Bronner, C. E., Bartlett, A. M., Whiteway, S. L., Lambert, D. C., Bennett, S. J., & Rabideau, A. J. (2013). An assessment of US stream compensatory mitigation policy: necessary changes to protect ecosystem functions and services. *Journal of the American Water Resources Association*, 49(2), 449-462.
- Brunner, G. W. (2016). *HEC-RAS, River Analysis System Hydraulic Reference Manual*. Davis, CA: US Army Corps of Engineers.
- Brunner, G. W. (2016). *HEC-RAS. River Analysis System User's Manual*. Version 5.0. Davis, CA: US Army Corps of Engineers.
- Buffington, J. M., & Montgomery, D. R. (1999). A procedure for classifying textural facies in gravel bed rivers. *Water Resources Research*, 35(6), 1903-1914.
- Burke, C. B., & Burke, T. T. (2015). *Stormwater drainage manual 2015*. West Lafayette, IN: Indiana Local Technical Assistance Program (LTAP) Publications.
- Cushing, C. E. & Allan, J. D., (2001). *Streams: their ecology and life*. San Diego, CA: Academic Press.
- Darby, S., & Sear, D. (Eds.). (2008). *River restoration: managing the uncertainty in restoring physical habitat*. John Wiley & Sons.
- Davidian, J. (1984). *Computation of water-surface profiles in open channels*. U. S. Geological Survey.
- Domeneghetti, A., Castellarin, A. & Brath, A. (2010). Effects of rating-curve uncertainty on the calibration of numerical hydraulic models. *First IAHR European Congress. Edinburgh*.
- Doyle, M. W., Dale E. Miller, D. E. & Jon M. Harbor, J.M. (1999). Should river restoration be based on classification schemes or process models? Insights from the history of geomorphology. *ASCE International Conference on Water Resources Engineering. ASCE: Seattle, Washington, USA (pp. 1-9)*.

- Doyle, M. W. & Shields, F. D. (2012). Compensatory mitigation for streams under the Clean Water Act: reassessing science and redirecting policy. *Journal of the American Water Resources Association*, 48(3), 494-509.
- Gore, J.A., (1985). *The restoration of rivers and streams*. Stoneham, MA: Butterworth Publishers.
- Hastie, L. C., Boon, P. J., & Young, M. R. (2000). Physical microhabitat requirements of freshwater pearl mussels, *Margaritifera margaritifera* (L.). *Hydrobiologia*, 429(1), 59-71.
- Hickey, J. T., Huff, R., & Dunn, C. N. (2015). Using habitat to quantify ecological effects of restoration and water management alternatives. *Environmental Modelling & Software*, 70, 16-31.
- Hicks, F.E. & Peacock, T. (2005). Suitability of HEC-RAS for flood forecasting. *Canadian Water Resources Journal*, 30(2), 159–174.
- Hoellein, T.J., Zarnoch, C.B., Bruesewitz, D.A., & DeMartini, J. (2017). Contributions of freshwater mussels (Unionidae) to nutrient cycling in an urban river: filtration, recycling, storage, and removal. *Biogeochemistry*, 135(3), 307-324.
- Ickes, B. S., Vallazza, J., Kalas, J. & Knights, B. (2005). *River floodplain connectivity and lateral fish passage: a literature review*. U.S. Geological Survey.
- Illinois Environmental Protection Agency. (2014). Illinois Integrated Water Quality Report and Section 303(d) List, 2014. *Illinois Environmental Protection Agency, Springfield, IL*.
- Illinois Tollway. (2014). Spring Brook Mitigation Site Report. *Illinois Tollway, Springfield, IL*.
- Knighton, A. D. (1999). Downstream variation in stream power. *Geomorphology*, 29(3), 293–306.
- Machtinger, E. T., Marks, R., Hohman, W., Butler, J., Patterson, M., Roe, K., Anderson, R. M., Koch, L. & Gullet, K. (2007.) Native freshwater mussels. *Fish and Wildlife Habitat Management Leaflet*. 46.
- Makaske, B. (2001). Anastomosing rivers: a review of their classification, origin and sedimentary products. *Earth-Science Reviews* 53(3), 149–196.
- Mays, L. W. (2010). *Water resources engineering*. Hoboken, NJ: John Wiley & Sons.
- Palmer, M. A. & Hondula, K. L. (2014). Restoration as mitigation: analysis of stream mitigation for coal mining impacts in southern Appalachia. *Environmental Science and Technology*, 48(18), 10552-10560.
- Palmer, M.A., Menninger, H.L. & Bernhardt, E. (2010). River restoration, habitat heterogeneity and biodiversity: a failure of theory or practice?. *Freshwater biology*, 55(s1), 205-222.
- Paver, N. & Olson A. (2017). Annual maintenance and monitoring report. Spring Brook No. 1 stream and wetland restoration project. WBK Engineering

- Riley, A. L., (1998). *Restoring streams in cities: A guide for planners, policymakers, and citizens*. Washington, DC: Island Press.
- Rinaldi M, & Johnson P.A. (1997). Stream meander restoration. *Journal of the American Water Resources Association*, 33(4), 855–866.
- Roni, P. & Beechie, T. (2013). *Stream and watershed restoration: a guide to restoring riverine processes and habitats*. West Sussex, UK: John Wiley & Sons, Ltd.
- Roni, P. & Quimby, E. (Eds.). (2005). *Monitoring stream and watershed restoration*. Bethesda, MD: American Fisheries Society.
- Sanz-Ronda, F. J., López-Sáenz, S., San-Martín, R., & Palau-Ibars, A. (2014). Physical habitat of zebra mussel (*Dreissena polymorpha*) in the lower Ebro River (Northeastern Spain): influence of hydraulic parameters in their distribution. *Hydrobiologia*, 735(1), 137-147.
- Sedlak, D. (2014). *Water 4.0: the past, present, and future of the world's most vital resource*. Yale University Press.
- Sefick, S. A., Kalin, L, Kosnicki, E, Schneid, B. P., Jarrell, M. S., Anderso, C. J., Paller, M. H. & Feminella, J. W. (2015). Empirical estimation of stream discharge using channel geometry in low-gradient, sand-bed streams of the southeastern plains. *Journal of the American Water Resources Association*, 51(4), 1060-107.
- Simon, A., Bennett, S.J. & Castro, J.M. eds., (2011). *Stream restoration in dynamic fluvial systems: scientific approaches, analyses, and tools* (Vol. 194). Washington, DC: American Geophysical Union.
- Simon, A., Doyle, M., Kondolf, M., Shields, F. D., B. Rhoads, B., & McPhillips, M. (2007). Critical evaluation of how the Rosgen classification and associated “natural channel design” methods fail to integrate and quantify fluvial processes and channel response. *Journal of the American Water Resources Association*, 43(5), 1117-1131.
- Sholtes J. S. and Doyle M. W. (2011). Effect of channel restoration on flood wave attenuation. *Journal of Hydraulic Engineering*, 137(2), 196-208.
- Society for Ecological Restoration International Science & Policy Working Group. (2004.) *The SER International Primer on Ecological Restoration*. Tucson, AZ: Society for Ecological Restoration International.
- SonTeck. (2016). *FlowTracker2 User's Manual*. San Diego, CA: SonTeck.
- Stuber, R. J., Gebhart, G., & Maughan, O. E. (1982). *Habitat suitability index models: green sunfish* (No. FWS/OBS-82/10.15). Fort Collins, CO: U.S. Fish and Wildlife Service.
- Turnipseed, D.P., & Sauer, V.B. (2010). *Discharge measurements at gaging station* (No. 3-A8). Reston, VA: U.S. Geological Survey.
- U.S. Water Resources Council. (1981). *Guidelines for determining flood flow frequency*. Reston, VA: Office of Water Data Coordination, U.S. Geological Survey.

Violin, C. R., Cada, P., Sudduth, E. B., Hassett, B. A., Penrose, D. L., & Bernhardt, E. S. (2011). Effects of urbanization and urban stream restoration on the physical and biological structure of stream ecosystem. *Ecological Applications*, 21(6), 1932–1949.

Waal, L.C. de, Large, A. R. G & Wade, P.M., (1998). *Rehabilitation of rivers: principles and implementation*. Chichester, England: John Wiley and Sons Ltd.

Walsh, C.J., Fletcher, T.D. & Ladson, A.R. (2005). Stream restoration in urban catchments through redesigning stormwater systems: looking to the catchment to save the stream. *Journal of the North American Benthological Society*, 24(30), 690-705.

Wohl, E., Angermeier, P. L., Bledsoe, B., Kondolf, G. M., MacDonnell, L., Merritt, D. M., Palmer, M. A., Poff, N. L., & Tarboton, D. (2005). River restoration. *Water Resources Research*, 41(10).

Wohl, E., Lininger, K.B., & Baron, J. (2017). Land before water: the relative temporal sequence of human alteration of freshwater ecosystems in the conterminous United States. *Anthropocene*, 18, 27–46.

YSI Incorporated. (2014). *EXO User Manual - Revision D*. Yellow Springs, OH: YSI Incorporated.

## APPENDIX

### Flow Frequency Analysis

A flow frequency analysis has been performed in order to determine the stream flow rates corresponding to various return periods, as means to simulate extreme flood events. The peak stage and discharge data (records from 1925 to 2008) was provided by WBK Engineering and collected by DuPage County at three different locations (upstream of Saint James Farm, 300 m downstream of Saint James Farm and upstream of Windfield Road).

Here, the Log Pearson Type III distribution is used to obtain the return period flow events. The first step in this method consists of determining the maximum flow rate for every year in the series ( $q_i$ ). Then, the logarithm of each selected value is computed ( $y_i = \log(q_i)$ ). The arithmetic average ( $\bar{y}$ ), standard deviation ( $s_y$ ) and skewness coefficient ( $C_s$ ) are calculated next for the series of  $y_i$  values. Now, the general expression for this distribution can be applied to determine the flow rates corresponding to each recurrence interval (Burke & Burke, 2015).

$$\log Q = \bar{y} + K_t s_y$$

where  $K_t$  is the frequency factor for the Log Pearson Type III distribution, which is tabulated for different skewness coefficients and recurrence interval values (Burke & Burke, 2015; U.S. Water Resources Council, 1981). The inverse logarithm of the previous expression gives the estimated maximum discharge. Figure 17 shows the estimated maximum discharge values for the analyzed recurrence intervals in logarithm scale.

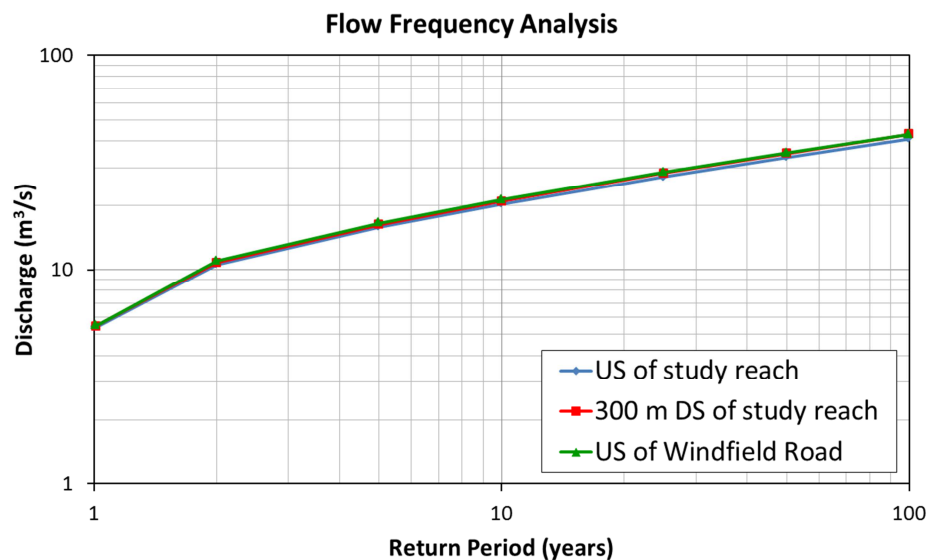


**Figure 17.** Return frequency analysis for Spring Brook determined at three different locations in the proximity of the restored reach. Information provided by WBK Engineering, LLC

The results observed in Figure 17 for the three data collection sites are very consistent. The average 1-year return flow event ( $5.45 \text{ m}^3/\text{s}$ ) is almost double the maximum flow rate manually measured in the field in May 2017 ( $2.53 \text{ m}^3/\text{s}$ ). The average 10-year and 100-year maximum flows are estimated to be  $20.83$  and  $42.26 \text{ m}^3/\text{s}$ .

**VITA**

**NAME:** Jose Javier Marquez Reina

**EDUCATION:** B.S., Agricultural Engineering, University of Seville, Seville, Spain, 2003  
M.S., Agronomic Engineering, University of Cordoba, Cordoba, Spain, 2008  
M.S., Civil Engineering, University of Illinois at Chicago, Chicago, Illinois, 2017

**PROFESSIONAL EXPERIENCE:** Research Assistant, Department of Civil and Materials Engineering, University of Illinois at Chicago, August 2016 – December 2017  
Dam Operations and Maintenance Manager, UTE DRAGADOS-GEOCISA & UTE Presas Sur, Cordoba, Spain, February 2010 – September 2013  
Occupational Health and Safety Supervisor, UPA-Andalucia, Seville, Spain, October 2009 – February 2010  
Engineering Consultant, Cordoba, Spain, February 2009 – March 2009  
Public Administration Assistant, Junta de Andalucia-DAP, Seville, Spain, October 2008 – December 2008

**PROFESSIONAL MEMBERSHIP:** American Society of Civil Engineers (ASCE)